Development of an ion beam measurement instrument for divertor simulation experiments in radio-frequency plasma

doi: 10.1063/5.0009321

Development of an ion beam measurement instrument for divertor simulation experiments in radio-frequency plasma

Cite as: AIP Advances **10**, 085018 (2020); https://doi.org/10.1063/5.0009321
Submitted: 01 April 2020 . Accepted: 01 July 2020 . Published Online: 17 August 2020

Hiroyuki Takahashi, Atsushi Okamoto, Sumio Kitajima, and Kenji Tobita

Development of an ion beam measurement instrument for divertor simulation experiments in radio-frequency plasma

Cite as: AIP Advances 10, 085018 (2020); doi: 10.1063/5.0009321
Submitted: 1 April 2020 • Accepted: 1 July 2020 •
Published Online: 17 August 2020

Hiroyuki Takahashi,[1,a)] Atsushi Okamoto,[2] Sumio Kitajima,[1] and Kenji Tobita[1]

AFFILIATIONS

[1] Department of Quantum Science and Energy Engineering, Tohoku University, 6-6-01-2 Aobayama, Sendai 980-8579, Japan
[2] Department of Energy Science and Engineering, Nagoya University Furo-cho, Chikusa-ku, Nagoya 464-8603, Japan

[a)] Author to whom correspondence should be addressed: hiroyuki.takahashi.c6@tohoku.ac.jp

ABSTRACT

A retarding field analyzer (RFA) that consists of three grids and a collector was developed, and the measurement of an ion beam that passes through plasma was demonstrated. First, a suitable grid potential structure to allow the measurement of an ion beam in plasma was investigated. After this investigation, a helium ion beam was measured without the production of plasma. It was found that the helium ion beam current was significantly overestimated when an unoptimized potential structure was utilized. One probable reason for the overestimation is secondary electron emission. Next, ion beam measurement in low density helium ionizing plasma was conducted. Accompanying the onset of the beam extraction, the collector current clearly increased, which implies that the beam ions penetrated through the plasma and reached the RFA. Subsequently, similar measurements were conducted after the electron density of the helium plasma was changed. Since a nearly identical beam extraction condition was retained, the ion beam current obtained after plasma production was almost constant. However, the ion beam current obtained during plasma production increased as the electron density increased. A calculation of the ion beam envelope indicated that space charge neutralization by bulk electrons could account for the increase in the ion beam current.

I. INTRODUCTION

In magnetic confinement fusion research, control of heat fluxes flowing onto divertor plates has been one of the most crucial problems yet to be solved. The formation of detached plasma is a promising method to handle enormous heat loads. Plasma volumetric recombination has an important role in detached plasma formation.[1] Plasma volumetric recombination has a high reaction rate at low electron temperatures and a high electron density region. Therefore, electron energy removal is important for forming and maintaining the detached plasma. However, especially in tokamak devices, edge localized modes (ELMs) associated with improved plasma confinement at the peripheral region periodically transport energetic plasma particles into the divertor region. There is a concern that pulsed heat loads could exceed the heat load limit of the divertor plates as the energy of the plasma particles, exhausted by ELM events, potentially rises to several keV. Therefore, a comprehensive understanding of the plasma volumetric recombination that coexists with energetic plasma inflow has been an important research topic.

Linear machines equipped with a direct current arc discharge plasma source have been contributing to investigate the subject by utilizing ELM-simulating electron pulses. For example, it has been asserted that energetic electrons injected into a detached helium plasma enhance ionization and excitation.[2] However, although energetic ions are also transported into the divertor region, their effect has not been clearly understood. In addition, before detached plasma, a relatively high temperature ionizing plasma is present. For these reasons, we have been conducting ion beam injection experiments on both ionizing and recombining plasma. Using helium ionizing plasma, it has been found that energetic ions spatially redistribute neutral particles through charge exchange (CX) momentum

transfer.[3] Experiments using helium recombining plasma indicated that the reaction rate of the volumetric recombination could be reduced by energetic ion collision.[4] The volumetric rates of particle extinction through collisions between energetic ions and target particles are given as $dn/dt = -\langle\sigma v\rangle n_i n_t$. $\langle\sigma v\rangle$, n_i, and n_t represent the rate coefficient of the ion collisions, density of the beam ions, and density of the target particles, respectively. Assuming that the beam ions are monoenergetic, $\langle\sigma v\rangle n_i n_t$ is proportional to the ion beam flux $n_i v_i$. However, the measurement of the ion beam flux was possible at only either the upstream or downstream edges, while it is well known that it would vary axially when the plasma density, neutral particle density, and magnetic field strength vary in the axial direction. In addition, since the bulk electrons that surround beam ions mitigate the space charge of beam ions, it is difficult to estimate the ion beam flux in plasma against that obtained in a vacuum. Therefore, the necessity arises for the *in situ* measurement of the ion beam flux in the target plasma.

Several toroidal plasma devices have demonstrated that the ion flux and ion energy can be obtained using a retarding field analyzer (RFA).[5–7] Therefore, in the present work, an RFA was developed to intercept the ion beam and was introduced to a radio-frequency plasma device. Since this paper reports on the initial results of the RFA, we mainly describe (1) the investigation of an optimal potential structure that allows ion beam measurement in plasma, (2) a demonstration of ion beam measurement in low density ionizing plasma, and (3) how bulk electrons affect ion beam transport. Details of the RFA are provided in Sec. II with the experimental setup. The experimental results using helium ionizing plasma and the helium energetic ion beam are presented in Sec. III and discussed in Sec. IV. This is followed by a summary in Sec. V.

II. EXPERIMENTAL SETUP AND RETARDING FIELD ANALYZER

In this section, the experimental setup for the energetic ion beam injection experiment is described. Subsequently, the design of the RFA that was introduced to the radio-frequency plasma source DT-ALPHA and the principle of energetic ion beam measurement using the RFA technique are presented.

A. Experimental apparatus

The ion beam injection experiment was performed using an RF plasma device DT-ALPHA.[8] Figure 1 shows a schematic of the DT-ALPHA device. The DT-ALPHA device consists of a quartz pipe and a vacuum chamber fabricated from stainless steel (SUS). The inner diameters of the quartz pipe and vacuum chamber are 36 mm and 63 mm, respectively. The z axis is defined as illustrated in Fig. 1. Two end-plates are installed at either end of the device. The upstream end-plate has a 10 mm aperture. A Faraday cup with an inner diameter of 8 mm is installed in front of the upstream end-plate. The downstream end-plate is divided into five segments in the radial and azimuthal directions. A gridded Faraday cup that is embedded in the central segment of the downstream end-plate can measure the ion beam flux that reaches the downstream end of the device. The inner diameter of the downstream Faraday cup is also 8 mm. An RF antenna is wound around the quartz pipe, and a matching circuit couples the power supply to the antenna. A 13.56 MHz RF discharge produces the plasma. The present experiment utilizes a low density helium ionizing plasma. Between z = 1.13 m and 1.43 m, two orifice units made of SUS are installed to control the axial distribution of neutral particles. The inner diameters of the orifice units are ~20 mm. In this experiment, the RFA was installed at z = 1.13 m. The electron temperature and electron density were obtained using a Langmuir probe (LP) installed at z = 0.98 m. The magnetic field strength and neutral helium pressure at z = 1.13 m were B = 0.16 T and p = 1.3 Pa–1.8 Pa, respectively. The upstream Faraday cup, Langmuir probe at z = 0.98 m, and RFA are radially movable.

A compact ion source is combined with the DT-ALPHA device at the upstream edge, as shown in Fig. 1. The plasma is produced by direct current arc discharge. The beam extraction system consists of the three electrodes, namely, acceleration, deceleration, and grounded electrodes. The ion beam transport is optimized by an einzel lens installed between the beam extraction system and the upstream end-plate. During the experiment, the acceleration voltage, arc current, and arc voltage were maintained at approximately V_{acc} = 10 kV–12 kV, I_{arc} = 3 A, and V_{arc} = 80 V, respectively. At the upstream Faraday cup, the typical ion beam current and beam current density are $I = 10^1$–10^2 μA and $j = 10^0$–10^1 A/m^2, respectively.

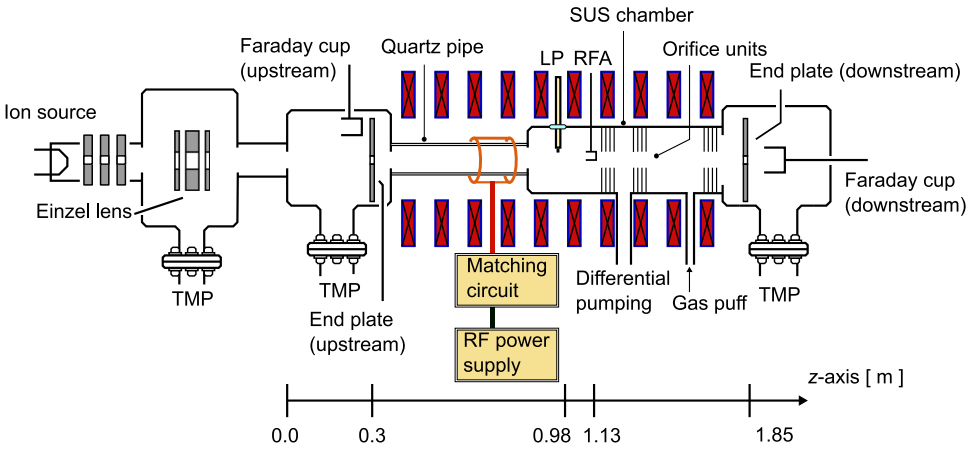

FIG. 1. Schematic of the DT-ALPHA device and an ion beam generator.

B. Retarding field analyzer

Figure 2(a) shows a schematic of the RFA developed in the present work. Usually, an RFA has four grids, but in the present study, a three-grid unit was applied to reduce the length. The grids were prepared from a molybdenum mesh (150 mesh/in.). The RFA collecting area was 8 mm in diameter. From the plasma facing grid, three grids are referred to as grid 3, grid 2, and grid 1, respectively. When designing the RFA, the heat load of the ion beam was not a crucial problem. For example, the heat load of an ion beam of $E_i = 10$ keV and $I = 10$ μA is less than 1 W. This value is small even if the extracted ion beam reaches the RFA without attenuation. However, there are two conflicting requirements. A smaller RFA is more suitable for reducing disturbances in plasma diagnostics, yet there is a possibility of breakdown if the grids are too close. Considering these requirements, the distance between two adjacent grids was determined to be 4 mm. The collector was fabricated from a SUS304 plate. The transparency of each grid was 0.68. Therefore, ~30% ($= 0.68^3$) of the beam ions are expected to reach the collector. The collector and grids were insulated from each other by an alumina tube. The electrostatic potentials of the collector and three grids could be controlled independently. One of the anticipated difficulties for applying the RFA technique to an RF device is a noise signal due to the oscillating field. The skin depth δ of an oscillating electric field is given as $\delta = \sqrt{\rho/\pi f \mu}$. Here, ρ, f, and μ represent the resistivity of the conductor, frequency of the oscillating field, and magnetic permeability of the conductor, respectively. The resistivity of SUS304 is $\rho = 7.2 \times 10^{-7}$ Ωm. The permeability is expected to be equal to that of free space because SUS304 is non-magnetic. Therefore, $\mu = 1.257 \times 10^{-6}$ Hm^{-1}. For $f = 13.56$ MHz, the skin depth is approximately $\delta \sim 0.12$ mm. The collector and grids are surrounded by a case fabricated from SUS304 to attenuate undesirable RF interference. The thickness of the case is 1 mm, so the amplitude of the oscillating electric field is expected to attenuate to 0.02%. To insulate the RFA from the plasma, the SUS case is surrounded by a ceramic cover. Except for the beam aperture, the front face of the RFA is covered by heat-resistant inorganic adhesives.

Figure 2(b) shows the principle of the RFA technique. The plasma-facing grid (grid 3) is maintained at a floating potential of ϕ_f to retard bulk electrons. Grid 2, being positively biased, retards bulk ions. Grid 1 is utilized to retard the tail components of the bulk electrons. Typical potentials of grid 1 and grid 2 were $\phi_{G1} = -350$ V and $\phi_{G2} = 50$ V, respectively. When the collector is bombarded with the ion beam, secondary electrons are emitted from the collector surface. However, the influence of secondary electron emission can be compensated when the potential of the collector is higher than the potential of the grid 1.

III. EXPERIMENTAL RESULTS

Initially, we investigated the optimal grid potential structure for reducing bulk plasma inflow. Subsequently, the helium energetic ion beam was superimposed onto the helium ionizing plasma, and the beam flux that passed through the plasma was measured.

A. Optimization of grid potential structure

Before conducting an ion beam injection experiment, a suitable grid potential structure to retard bulk plasma inflow was investigated. The electron temperature and electron density near the plasma production region were $T_e = 3.5$ eV and $n_e = 5.0 \times 10^{16}$ m^{-3}, respectively. Figure 3 shows the collector current I_c as a function of the potential of the grid 1. The circles, squares, and triangles correspond to $\phi_{G2} = -20$ V, 0 V, and 20 V, respectively. Here, ϕ_{G2} is the potential of grid 2. The potential of the collector ϕ_c was maintained at 0 V. Grid 3, which faced the plasma, was maintained at the floating potential. The inset in Fig. 3 is an enlarged view around $\phi_{G1} \leq -250$ V. As shown in Fig. 3, I_c has a negative value in the region where ϕ_{G1} is insufficient, thus indicating that electrons can reach the collector. However, I_c approached zero as ϕ_{G1} negatively increased, and finally neared zero at $\phi_{G1} = -350$ V. This tendency indicates that grid 1 effectively retarded bulk electrons by forming a retarding field. As shown in the inset of Fig. 3, I_c at $\phi_{G1} = -350$ V in the case of $\phi_{G2} = 20$ V is nearly zero, while the other two potential cases show a positive current of 0.02 mA. Using $T_e = 3.5$ eV and $n_e = 5 \times 10^{16}$ m^{-3}, the ion current flux at the

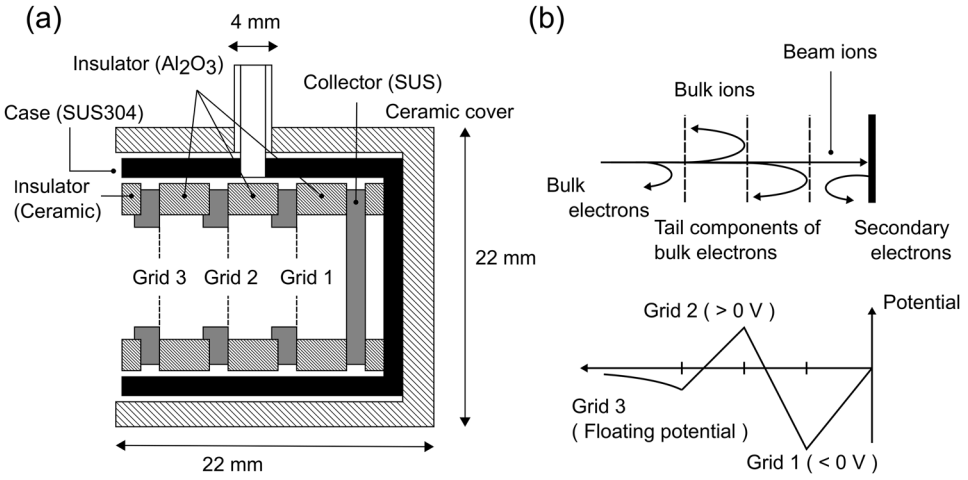

FIG. 2. Schematics of the (a) retarding field analyzer and (b) potential structure for ion beam measurement.

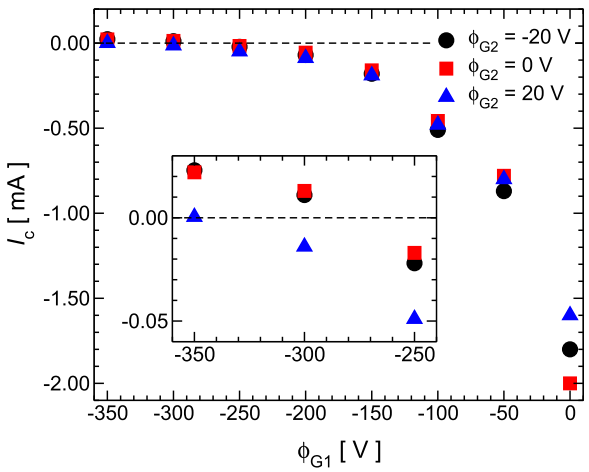

FIG. 3. Collector current as a function of potential of grid 1. Circles, squares, and triangles correspond to $\phi_{G2} = -20$ V, 0 V, and 20 V, respectively. Potentials of grid 3 and the collector were ϕ_f and 0 V. During this investigation, no ion beam was injected.

sheath edge of grid 3 is evaluated as $j = 75$ A/m^2. At $\phi_{G2} = -20$ V and 0 V, the ions inside the RFA are estimated to travel roughly in the absence of a strong electric field. Therefore, the ion current of $I = j \times S \times \eta^3 = 1.1$ mA is expected to reach grid 1. Here, S and η represent the grid surface area and grid transparency, respectively. If this ion current is conserved between grid 3 and the collector, 1.1 mA is expected to be measured at the collector. However, the measured ion current was 0.02 mA. This indicates that the experimental ion transmission rate was much lower than that expected from the geometric structure. An interpretation of this discrepancy is attempted in terms of the space charge effect. Assuming that the ion current density $j = 75$ A/m^2 and sheath potential $V_{sh} = -20$ V, we solved the ion beam envelope equation. Here, $V_{sh} = -20$ V is slightly deeper than the potential drop inside the sheath ($3.83T_e = 13.4$ V), but not very different. By solving the equation, the evolution of the ion envelope along the axial direction can be obtained. First, we apply 4 mm as the initial ion radius (r_0) because the geometric radius of the collecting area is 4 mm. It was found that ions rapidly diverge inside the RFA when this value was assumed. Conversely, when $r_0 = 0.3$ mm was used, the ion beam radius at the collector position (12 mm behind the grid 3) became ~4 mm. This implies that almost all the ions reach the collector even though they radially diverge inside the RFA volume. In this case, $(0.3/4)^2 = 0.006$ of the sheath edge ion current reaches the collector. As described above, $I = 1.1$ mA is expected at the sheath edge of grid 3 and 0.02 mA is the experimentally observed collector current. The ratio of these two currents is 0.02/1.1 = 0.018. This value is thrice the one above. Here, it should also be considered that grid 1, being negatively biased, could function as an electrostatic lens and focus ions on the collector. This effect reduces the ion footprint at the collector, with more ions reaching the collector than the calculation predicts. When the inner wall (Al_2O_3 insulator) of the RFA is bombarded by the diverged ions, secondary electrons are emitted from the surface. The number of secondary electrons will decrease when the negative bias of grid 1 increases because the bombardment of the inner wall is reduced. Therefore, as well as the bulk electron repulsion by the potential of grid 1, the reduction of secondary electron emission would also contribute to the tendency of the collector current to increase against the potential of grid 1. An investigation of the axial electric field formed around the grids could provide a deeper understanding of this phenomenon; however, that is not the main objective of this study.

As shown in Fig. 3, a high potential like −350 V is necessary to retard bulk electrons, but this value seems to be extremely high when the electron temperature is considered. In RF plasmas, especially capacitively coupled plasma (CCP), the RF components of the plasma potential can be large. This fact could explain the necessity of the negatively large ϕ_{G1}. Although it is difficult to determine the discharge mode, the target plasma was possibly a CCP because $n_e = 5 \times 10^{16}$ m^{-3} is in the typical n_e range of CCP discharges.

B. Ion beam measurement in ionizing plasma

It is confirmed that an optimal potential structure successfully retards bulk plasma inflow. Subsequently, the energetic helium ion beam ($E_i = 10$ keV) was measured using the RFA. During this measurement, the helium neutral pressure was $p = 1.3$ Pa. Figure 4 shows the time evolution of the collector current. Note that I_c in Fig. 4(a) was obtained without plasma production, whereas that in Fig. 4(b) was obtained during plasma production. In Fig. 4(b), the helium plasma was produced from $t = 0$ s to $t = 5.2$ s. The same magnetic configuration and neutral pressure were utilized in both measurements. The potentials of grids 1 and 2 in the "biased case" were

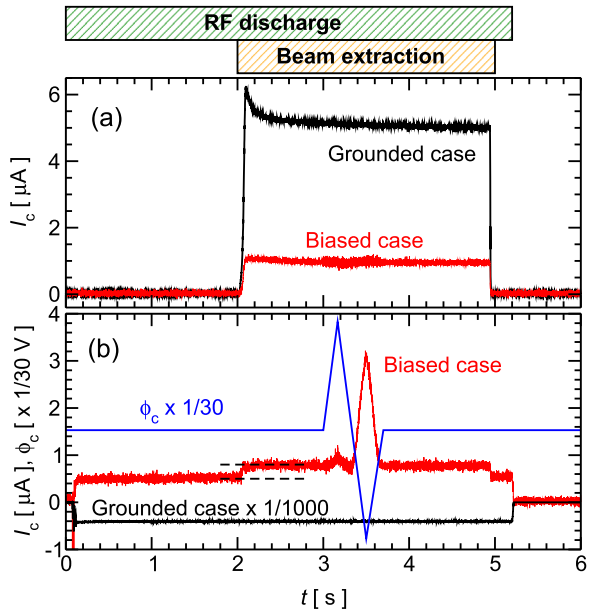

FIG. 4. Time evolution of the collector current I_c measured (a) without plasma and (b) with plasma. Potentials of grid 1 and grid 2 in "biased case" were $\phi_{G1} = -350$ V and $\phi_{G2} = 50$ V, respectively, while both grids were grounded in the "grounded case." In both cases, grid 3 was maintained at the floating potential. The collector potential was swept from −25 V to 120 V in the "biased case." The helium neutral pressure was $p = 1.3$ Pa.

$\phi_{G1} = -350$ V and $\phi_{G2} = 50$ V, respectively. Conversely, grids 1 and 2 were grounded in the "grounded case." In both cases, grid 3 was maintained at the floating potential. In the "grounded case," the collector was also grounded. It is expected that the collector current is independent of the collector potential when the bulk plasma inflow is completely suppressed. To confirm this, in the "biased case" of Figs. 4(a) and 4(b), the potential of the collector was swept between -25 V $< \phi_c <$ 120 V.

As shown in Fig. 4(a), an ion beam current of ~1 μA was obtained in the biased case. However, for the grounded case, it was ~5 μA. In the biased case, the secondary electrons emitted from the collector are expected to return to the collector because ϕ_c is always larger than ϕ_{G1}. Conversely, the influence of secondary electron emission would be non-negligible when the collector is grounded. The collector current for each case would be written as

$$I_c^B = qS_c\Gamma_i, \tag{1}$$

$$I_c^G = qS_c[(1 + \zeta)\Gamma_i + \zeta\Gamma_n]. \tag{2}$$

Superscripts "B" and "G" represent the biased and grounded cases, respectively. q, S_c, and ζ represent the charge of the beam ions, surface area of the collector, and secondary electron emission coefficient, respectively. Γ_i and Γ_n are the ion beam flux and the charge-exchanged neutral beam flux that reach the collector. Here, the ζ of the ion beam and the neutral beam are assumed to be equal. In the DT-ALPHA device, it was shown that the neutral beam flux produced by the charge exchange momentum transfer was twice or thrice greater than the ion beam flux.[9] Although neutral pressure in the present experiment was greater than that in Ref. 9, $\Gamma_n = 2$–$3 \times \Gamma_i$ is assumed here. Reference 9 also indicates that the secondary electron emission coefficient of the SUS is $\zeta = 1$–2. Therefore, I_c^G can be estimated as $I_c^G = 4$–$9 I_c^B = 4\ \mu$A–9 μA. This is almost the same value as the experimental result shown in Fig. 4(a). This indicates that the possible reason for the difference in I_c between the two cases is the presence of secondary electrons.

The helium ion beam was then superimposed onto a helium ionizing plasma. The electron temperature and electron density of the target plasma were $T_e = 7.7$ eV and $n_e = 1.1 \times 10^{16}$ m^{-3}, respectively. In Fig. 4(b), the collector current in the grounded case is also plotted for reference. In the grounded case, the collector current has a negative value, implying that bulk electrons had reached the collector. Conversely, in the biased case, I_c has a positive value at every position. This indicates that the bulk electron inflow was mitigated. During $t = 0$ s–2 s, a collector current of ~0.5 μA was observed. This would be due to the bulk ion inflow because in this period, there was no ion beam. Accompanying the onset of the beam injection, the collector current clearly increased to 0.8 μA and then decreased to 0.5 μA after the beam was removed. The ion beam current passing through the target plasma was, therefore, 0.3 μA. As shown in Fig. 4(a), the ion beam current obtained without the production of plasma was ~1 μA. While an RF field was applied to produce plasma in Fig. 4(b), the data in Fig. 4(a) were obtained without the RF field. However, the influence of an RF field on ion beam current is negligible because the RF antenna is placed ~1 m behind the ion source. In addition, I_c showed a sudden peak at $t = 3.5$ s. However, we do not have a clear understanding of what caused this peak.

C. Dependence of ion beam current on bulk electrons

To investigate the influence of bulk electrons on ion beam transport, similar experiments were performed with electron densities varying from 3.1×10^{15} m^{-3} to 1.6×10^{17} m^{-3}. In this case, the helium neutral pressure was $p = 1.8$ Pa. As the electron density increased, the electron temperature slightly decreased from $T_e = 5.3$ eV to 3.3 eV. Similarly to Fig. 4, each grid was maintained at $\phi_{G1} = -350$ V, $\phi_{G2} = 50$ V, and $\phi_{G3} = \phi_f$, respectively. The collector potential was swept from -20 V to 120 V, as shown in Fig. 5(a). Figure 5(b) shows the time evolution of the collector current at $n_e = 3.6 \times 10^{16}$ m^{-3}. The energy of the beam ions was 12 keV. At approximately $t = 4$ s–5 s, a collector current of ~0.2 μA was observed. This is the value of the ion beam current that reached the RFA without bulk plasma because no RF power was applied in this period. Hereafter, this current is referred to as I_0. In contrast with Fig. 4, the vertical axis of Fig. 5 has negative values during plasma production, indicating that the bulk electrons were not retarded completely. This implies that grid 1 should be more negatively biased to suppress the bulk electron inflow at this electron density. However, the accompanying increase in the collector current still can be clearly observed with the onset of the beam extraction. I_c was almost -1.1 μA until $t = 2$ s, but it increased to -0.9 μA from $t = 2$ s. The increase in the collector current ΔI is comparable to the collector current obtained after RF discharge, $\Delta I \sim I_0$.

The dependence of the ion beam current on electron density is summarized in Fig. 6. The beam ion energy was kept at $E_i = 12$ keV. For reference, I_0 and $\Delta I/I_0$ obtained from Fig. 4 are also shown as open squares. Figure 6(a) shows the beam current I_0 as a function

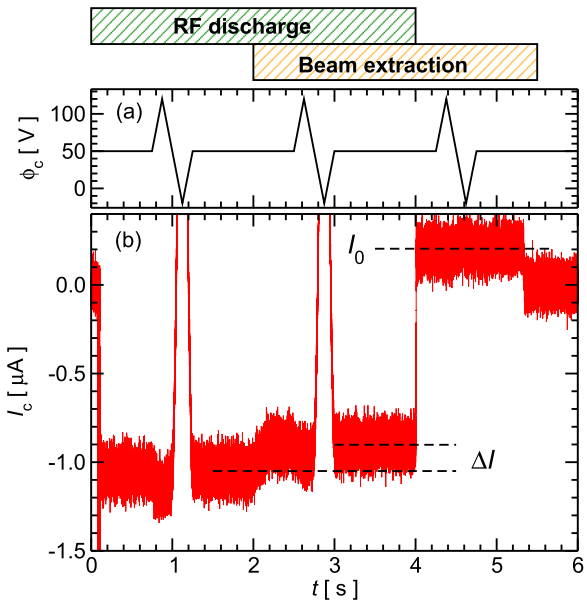

FIG. 5. Time evolution of the (a) collector potential ϕ_c and (b) collector current I_c. The electron temperature and electron density of the target plasma were $T_e = 5.0$ eV and $n_e = 3.6 \times 10^{16}$ m^{-3}, respectively. The potentials of each grid were $\phi_{G1} = -350$ V, $\phi_{G2} = 50$ V, and $\phi_{G3} = \phi_f$. The helium neutral pressure was $p = 1.8$ Pa.

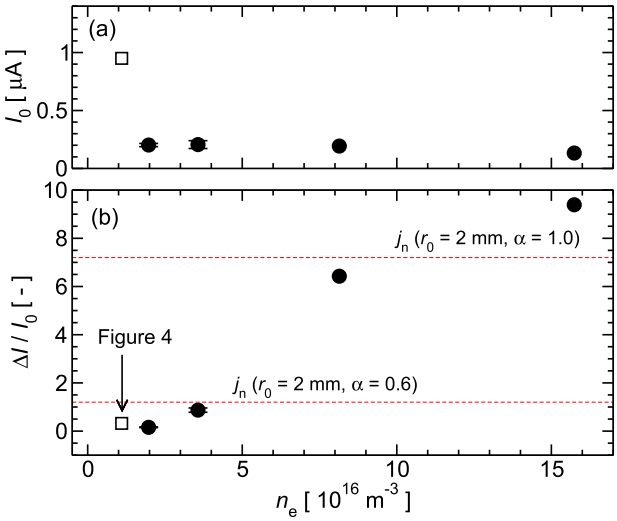

FIG. 6. (a) Ion beam current obtained after plasma production I_0 and (b) $\Delta I/I_0$ as a function of the electron density. The beam energy of filled circles is E_i = 12 keV. For reference, I_0 and $\Delta I/I_0$ obtained from Fig. 4 are also shown as open squares. The helium neutral pressure was p = 1.8 Pa. The two dashed lines represent the normalized ion beam current density calculated from the beam envelope equation.

of n_e. In the case of E_i = 12 keV, I_0 shows an almost constant value because this value was obtained after the RF discharge. Even though the difference in the ion beam energy between the two cases is small, the I_0 of the open square is much larger than that of the filled circles. A possible reason for this result was the difference in beam focusing conditions. Figure 6(b) shows $\Delta I/I_0$ as a function of the electron density of the target plasma. As described above, I_0 at E_i = 12 keV was almost constant. However, $\Delta I/I_0$ clearly differs for electron density. $\Delta I/I_0$ was almost equal to 1 at n_e = 3.6 × 10^{16} m^{-3}, and exceeded 1 as n_e increased. Conversely, it was less than 1 in the relatively lower density case. These results indicate that ion beam transport in plasma is strongly affected by the bulk plasma. In Sec. IV, the $\Delta I/I_0$ dependence on electron density is discussed in terms of the divergence of the beam ions. The two dashed lines in Fig. 6(b) are explained in detail in Sec. IV.

IV. DISCUSSIONS

In principle, beam ions radially diverge owing to their radial electric field E_r. E_r formed around an ion beam flux surface is expressed as[10]

$$E_r = \frac{1}{2\pi r\varepsilon_0}\frac{I_b}{\sqrt{2qV_{acc}/m_i}}. \quad (3)$$

Here, r and I_b represent the beam radius and beam current, respectively. V_{acc} represents the acceleration voltage. In plasma, beam ions are surrounded by bulk electrons and their radial electric field is mitigated. To consider this effect qualitatively, we introduced the term α (=0–1) into Eq. (3). Hereafter, the radial electric field of the beam ions in plasma is calculated as $(1-\alpha)\times E_r$. α = 1 implies that the radial electric field is completely suppressed by bulk electrons. Conversely, α = 0 implies that the bulk electrons have no effect. The equation to describe the motion of beam ions is written as

$$m_i\frac{d^2r}{dt^2} = qE_r. \quad (4)$$

Assuming that $dz/dt \sim v_i$, the left-hand side of Eq. (4) becomes $m_i v_i^2 d^2r/dz^2$. Here, v_i is the velocity of the beam ion. Using Eqs. (3) and (4), the axial distribution of the beam radius $r(z, \alpha)$ can be obtained. When we also assume that the ion beam current I_b is conserved, the beam current density j_i can be calculated as $j_i = I_b/\pi r^2$. Neutralization of the ion beam space charge by bulk electrons could decrease the ion beam radius, producing an increase in the ion current greater than in the absence of plasma. A larger α corresponds to a higher electron density, whereas a smaller α corresponds to a lower electron density or background gas condition. When the ion beam current density at the background gas condition is referred to as j_i^0, the extent of increase in the current density by neutralization is expressed as j_i/j_i^0. Therefore, the influence of space charge neutralization can be investigated by comparing the experimentally obtained $\Delta I/I_0$ and the numerically evaluated j_i/j_i^0. Hereafter, this current density ratio j_i/j_i^0 is referred to as j_n. It should be noted that the value of α would not be zero even if the plasma were not produced because the ion beam space charge was neutralized by the background gas. Therefore, we assumed that the background gas condition corresponds to α = 0.5. Using I = 35 μA and r_0 = 2 mm as the initial ion beam current and ion beam radius, the dashed lines shown in Fig. 6(b) were obtained. At α = 0.6, j_n becomes ~1.2. This value is close to $\Delta I/I_0$ at n_e = 3.6 × 10^{16} m^{-3}. When α increases to 1.0, j_n increases to ~7, which is similar to $\Delta I/I_0$ at n_e = 8.1 × 10^{16} m^{-3}. This comparison indicates that the experimental results ($\Delta I/I_0 > 1$) could be understood from the neutralization of the ion beam space charge. Conversely, this cannot explain the experimental results of $\Delta I/I_0$ being below 1 that was obtained at the relatively lower electron density region. To develop an understanding of this result would be the substance of a future research project.

Evaluations of beam charge states and their axial profiles are important for discerning the ion beam current described in Sec. III. For simplicity, ion beams that pass through background gases were considered here. We approximately calculated the axial profiles of a helium ion beam flux (Γ_i) and a fast helium atom beam flux (Γ_n) produced by charge exchange (CX) interactions. Ion impact ionization processes were ignored because these cross sections are much smaller than those in CX interactions. In addition, space charge neutralization due to electrons produced by ion impact ionization was ignored. Under these conditions, the time derivatives of the beam ion density (n_i) and fast helium atom density (n_0^F) are described as

$$\frac{dn_i}{dt} = v_i\frac{dn_i}{dz} - n_i n_0^S\langle\sigma_{CX}v_i\rangle, \quad (5)$$

$$\frac{dn_0^F}{dt} = v_0\frac{dn_0^F}{dz} + n_i n_0^S\langle\sigma_{CX}v_i\rangle. \quad (6)$$

Here, v_i, v_0, n_0^S, and σ_{CX} represent the velocity of beam ions, velocity of charge-exchanged fast neutrals, density of background helium atoms, and cross section of the CX interaction, respectively. v_0 was assumed to be equal to v_i. For the CX cross section, σ_{CX} = 5.5 × 10^{-20} m^2 was utilized. n_0^S was evaluated from neutral pressure. For simplicity, spatially uniform neutrals were assumed. In the case of

Fig. 4(a), the neutral pressure at the RFA region was p = 1.3 Pa, but the averaged pressure between the upstream end-plate ($z \sim 0.3$ m) and the RFA (z = 1.13 m) would be smaller than this value because a turbo molecular pump was placed at the upstream end of the device. Therefore, we utilized p = 1.0 Pa and 0.5 Pa and calculated the axial profiles of Γ_i and Γ_n. When p = 1.0 Pa and T = 300 K were assumed, Γ_i at the RFA position became several orders of magnitude smaller than that at z = 0.3 m. This cannot explain the experimental result because an ion beam current of ~1 μA was observed, as shown in Fig. 4(a). Instead, when p = 0.5 Pa and T = 400 K were considered, Γ_i at z = 1.13 m became 1/60 of that at z = 0.3 m. As described in Sec. II A, the typical ion beam current observed by the upstream Faraday cup was $I = 10^1\ \mu A$–$10^2\ \mu A$. Since 1 μA was observed in the experiment, the ion beam ratio between the two positions is 1/100–1/10, which is ~1/60. Therefore, it seems that the ion beam current shown in Fig. 4(a) could be interpreted using this consideration. To obtain a deeper understanding, we need to investigate the neutral pressure distribution and neutral temperature.

V. CONCLUSION

A retarding field analyzer consisting of three grids and a collector was introduced into the radio-frequency plasma source DT-ALPHA. Using helium ionizing plasma, an optimal grid potential structure to reduce bulk plasma inflow was investigated. When the grid potential was not optimized, a slight positive current was observed. This value was much smaller than expected from the ion current flux, grid surface area, and grid transparency. The decrease in the ion transmission rate due to the space charge effect may be a possible reason. Measurements of an energetic helium ion beam were then conducted. First, the ion beam was measured without the production of plasma. The results indicated that the ion beam current was significantly overestimated owing to secondary electrons when an unoptimized potential structure was utilized. When an optimized grid potential was utilized, an ion beam of 1 μA was measured. To interpret this value, the axial profiles of the ion beam and neutral beam fluxes were calculated. This calculation indicated that the observed beam current could be interpreted by the CX interaction. However, further investigation of the background neutral particle profile and temperature is required for a more detailed understanding of the result. Thereafter, beam injection into the helium ionizing plasma was conducted. The collector current clearly increased accompanying the onset of beam extraction, which confirms the *in situ* measurement of the ion beam in plasma. Maintaining a nearly identical beam extraction condition, the ion beam current was measured by changing the electron density to investigate how the bulk plasma affects ion beam transport. Although the beam current I_0 was similar, $\Delta I/I_0$ seemed to depend on the electron density. To investigate whether or not this trend can be interpreted as space charge neutralization by bulk electrons, the ion beam envelope was numerically calculated. Although the initial ion beam radius and space charge compensation parameter should be assumed, an increase in the compensation parameter due to an increase in n_e would explain the experimental trend of $\Delta I/I_0$.

ACKNOWLEDGMENTS

The authors are grateful to Mr. D. Nakamura for his technical support. This work was partly supported by the Japan Society for the Promotion of Science (JSPS) Grants-in-Aid for Scientific Research (KAKENHI) for Young Scientists (B) (Grant No. 17K14895) and Grants-in-Aid for Scientific Research (B) (Grant No. 20H01883).

DATA AVAILABILITY

The data that support the findings of this study are available from the corresponding author upon reasonable request.

REFERENCES

[1] S. I. Krasheninnikov, A. Y. Pigarov, D. A. Knoll, B. LaBombard, B. Lipschultz, D. J. Sigmar, T. K. Soboleva, J. L. Terry, and F. Wising, Phys. Plasmas **4**, 1638 (1997).
[2] N. Ohno, D. Nishijima, S. Takamura, Y. Uesugi, M. Motoyama, N. Hattori, H. Arakawa, N. Ezumi, S. Krasheninnikov, A. Pigarov, and U. Wenzel, Nucl. Fusion **41**, 1055 (2001).
[3] A. Okamoto, H. Takahashi, S. Kitajima, and M. Sasao, Plasma Fusion Res. **6**, 1201153 (2011).
[4] H. Takahashi, A. Okamoto, D. Nakamura, T. Miura, P. Boonyarittipong, and S. Kitajima, Phys. Plasmas **23**, 112510 (2016).
[5] R. A. Pitts, W. Fundamenski, S. K. Erents, Y. Andrew, A. Loarte, C. Silva, and JET-EFDA Contributors, Nucl. Fusion **46**, 82 (2006).
[6] M. Kočan, A. Herrmann, H. W. Müller, V. Rohde, T. Eich, M. Bernert, S. Carpentier-Chouchana, J. P. Gunn, A. Kirk, M. Komm, R. A. Pitts, and ASDEX team, Plasma Phys. Controlled Fusion **53**, 065002 (2011).
[7] P. Tamain, M. Kočan, J. Gunn, A. Kirk, J.-Y. Pascal, and M. Price, J. Nucl. Mater. **415**, S1139 (2011).
[8] A. Okamto, K. Iwazaki, T. Isono, T. Kobuchi, S. Kitajima, and M. Sasao, Plasma Fusion Res. **3**, 059 (2008).
[9] A. Okamoto, T. Isono, T. Nishiuchi, H. Takahashi, S. Kitajima, and M. Sasao, Plasma Fusion Res. **5**, S2088 (2010).
[10] A. D. Stepanov, E. P. Gilson, L. R. Grisham, I. D. Kaganovich, and R. C. Davidson, Phys. Plasmas **23**, 043113 (2016).